Molecular-Fluorescence Enhancement via Blue-Shifted Plasmon-Induced Resonance Energy Transfer

Mingsong Wang,[†] Bharath Bangalore Rajeeva,[‡] Leonardo Scarabelli,[∥] Evan P. Perillo,[§] Andrew K. Dunn,[§] Luis M. Liz-Marzán,[∥,¶,⊥] and Yuebing Zheng*,[†,‡]

[†]Department of Mechanical Engineering, [‡]Materials Science & Engineering Program and Texas Materials Institute, and [§]Department of Biomedical Engineering, The University of Texas at Austin, Austin, Texas 78712, United States

[∥]Bionanoplasmonics Laboratory, CIC biomaGUNE, Paseo de Miramón 182, 20009 Donostia, San Sebastián, Spain

[¶]Ikerbasque, Basque Foundation for Science, 48013 Bilbao, Spain

[⊥]Biomedical Research Networking Center in Bioengineering, Biomaterials, and Nanomedicine, CIBER-BBN, 20009 Donostia, San Sebastián, Spain

S *Supporting Information*

ABSTRACT: We report molecular-fluorescence enhancement via the blue-shifted plasmon-induced resonance energy transfer (PIRET) from single Au nanorods (AuNRs) to merocyanine (MC) dye molecules. The blue-shifted PIRET occurs when there is a proper spectral overlap between the scattering of AuNRs and the absorption of MC molecules. Along with the quenching of scattering from AuNRs, the blue-shifted PIRET enhances the fluorescence of nearby molecules. On the basis of the fluorescence enhancement, we conclude that AuNRs can be used as donors with clear advantages to excite the fluorescence of molecules as acceptors in AuNR–molecule hybrids. On the one hand, compared to conventional molecular donors in Förster resonance energy transfer (FRET), AuNRs have much larger absorption cross sections at the plasmon resonance frequencies. On the other hand, energy-transfer efficiency of PIRET decreases at a lower rate than that of FRET when the donor–acceptor distance is increased. Besides, the blue-shifted PIRET allows excitation with incident light of lower energy than the acceptor's absorption, which is difficult to achieve in FRET because of the Stokes shift. With the capability of enhancing molecular fluorescence with excitation light of low intensity and long wavelength, the blue-shifted PIRET will expand the applications of nanoparticle–molecule hybrids in biosensing and bioimaging by increasing signal-to-noise ratio and by reducing photodamage to biological cells and organelles at the targeted areas.
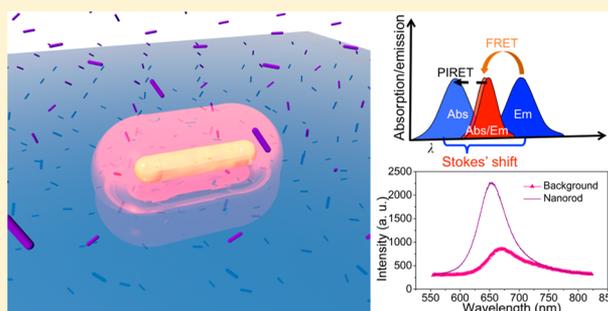
INTRODUCTION

Surface plasmon energy can be transferred from Au nanoparticles (AuNPs) as donors to dye molecules or semiconductors as acceptors, through so-called plasmon-induced resonance energy transfer (PIRET) or plasmon resonance energy transfer (PRET).[1−7] Compared with dye molecule donors in Förster resonance energy transfer (FRET), AuNP donors in PIRET have advantages toward applications in biosensing and bioimaging with two main aspects. First of all, AuNP donors require incident light with lower intensity to excite acceptors than that required for dye molecule donors. AuNPs not only have larger absorption cross sections than dye molecules (4−5 orders of magnitude larger than that of conventional dyes) because of the excitation of surface plasmons,[8−10] but additionally, the energy-transfer efficiency of PIRET decays more slowly when the NP−molecule distance is increased, as compared to FRET.[11,12] Therefore, NP−molecule hybrids are promising candidates for biosensing and

bioimaging with low-power excitation and high signal-to-noise ratio.

The second advantage of PIRET is its ability to enhance molecular fluorescence using excitation light with longer wavelength (i.e., lower energy) than that of the molecular absorption peak. We thus define the PIRET with excitation at the longer wavelength regime of molecular absorption as blue-shifted PIRET. In contrast, because of the Stokes shift, FRET often occurs when the absorption peak wavelength of the donor is shorter than that of the acceptor, and there is an overlap between the emission spectrum of the donor and the absorption spectrum of the acceptor (Figure 1a).[4] Such a requirement on the peak wavelengths limits the choices of fluorophore pairs that exhibit FRET. Stokes shift does not occur in metal NPs since the radiative decay of localized surface
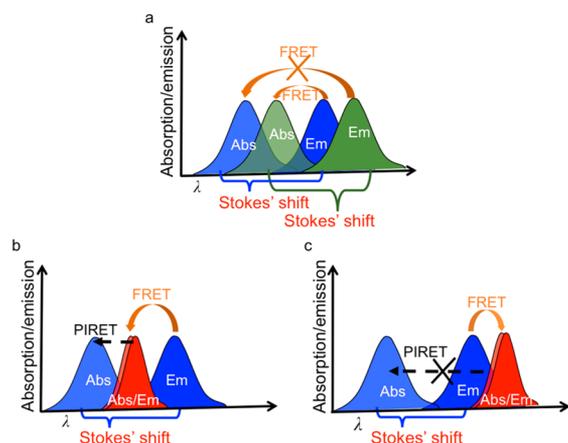
Figure 1. Schematics of different energy transfer scenarios in NP−molecule hybrids. (a) Scheme showing energy transfer between a pair of fluorophores. Because of Stokes shift, the emission of an acceptor (green) does not overlap with the absorption of a donor (blue) and FRET does not occur between them. The partial overlap between the emission of the donor (blue) and the absorption of the acceptor (green) leads to FRET from donor to acceptor. (b) Scheme of energy transfer between fluorophores and AuNPs. No obvious Stokes shift occurs to the LSPR-associated absorption and emission spectra of AuNPs (red). As expected, FRET from fluorophores to AuNPs occurs because of the spectral overlap between dye fluorescence (blue) and AuNP absorption. We demonstrate here that PIRET from AuNPs to fluorophores can occur to enhance the molecular fluorescence even if the absorption peak wavelength of the AuNPs is longer than that of fluorophores. PIRET is contingent upon a spectral overlap between the scattering/emission of AuNPs and the absorption of fluorophores, as further described in c. (c) Scheme showing energy transfer between fluorophores and AuNPs. When there is no spectral overlap between the scattering of AuNPs and the absorption of fluorophores, PIRET does not occur. FRET from fluorophores to AuNPs occurs because of the spectral overlap between dye fluorescence and AuNP absorption.

plasmon resonances (LSPRs) occurs earlier than nonradiative relaxation, leading to a strong overlap between the absorption and scattering spectra of the NPs. Therefore, as shown in Figure 1b, there is a good chance for an overlap between the scattering spectrum of a metal NP and the absorption spectrum of a fluorophore, enabling the blue-shifted PIRET from the NP to the molecule fluorophore.[4]

Despite their clear advantages in biosensing and bioimaging via the use of low-energy, low-intensity light, the application of AuNPs as donors in blue-shifted PIRET has not been demonstrated experimentally. In previous studies, the effect of PIRET has been limited to dips in the scattering spectra of metal NPs.[1−3] We report herein the first demonstration of the enhancement of molecular fluorescence via blue-shifted PIRET from single Au nanorods (AuNRs) to molecule fluorophores, which indicates that AuNPs as donors can enhance the fluorescence excitation of dye molecule acceptors.

■ EXPERIMENTAL SECTION

Sample Preparation. Solutions of Au nanorods (AuNRs, Alfa Aesar) were drop-coated on microscope calibration slides (AmScope) and dried naturally. We used AuNRs with three different sizes: 12−18 nm diameter × 49−59 nm length, 19−25 nm diameter × 50−60 nm length, and 19−25 nm diameter × 63−73 nm length. A Hitachi S-5500 scanning electron microscope (SEM) was used to measure the morphology of AuNRs. We mixed spiropyran (SP, Sigma-Aldrich) and poly(methyl methacrylate) (PMMA, Sigma-Aldrich) with a weight ratio of 2:1 (8 wt %:4 wt %) in chlorobenzene to prepare PMMA films with a high concentration of SP molecules. The SP-doped PMMA films were spin-coated onto the microscope slides with AuNRs. The spin coater (Laurell Technologies) was set as 2000 rpm and was run for 1 min. The thickness of the SP-doped PMMA film was measured as ∼580 nm by a Wyko NT9100 Optical Profilometer (Veeco Instruments Inc.).

Optical Measurements. A dark-field microscope (Ti-E inverted microscope, Nikon) with a halogen white light source (12 V, 100 W) was employed to measure the scattering spectra of single AuNRs and the white-light-excited fluorescence of merocyanine (MC) molecules. A mercury light source (C-HGFIE, Nikon) with excitation filters was used to generate UV light (DAPI shift filter set, excitation: 358 nm). We used markers on microscope calibration slides to locate single AuNRs. UV light was applied to convert molecules from SP to MC isomers. We used an oil-immersion dark-field condenser in conjunction with 100× objective for single-nanoparticle spectroscopy. In some cases, a 665 nm long-pass filter was placed on the top of the condenser to partially block the white light at the shorter wavelengths.

Fluorescence lifetime imaging microscopy (FLIM) was performed using time-correlated single-photon-counting (TCSPC) technique. The major components of FLIM setup include a femtosecond titanium:sapphire laser tuned to 800 nm (≈200 fs) (Mira 900, Coherent), galvo scanning mirrors (6215H, Cambridge Tech.), and a GaAsP photomultiplier tube
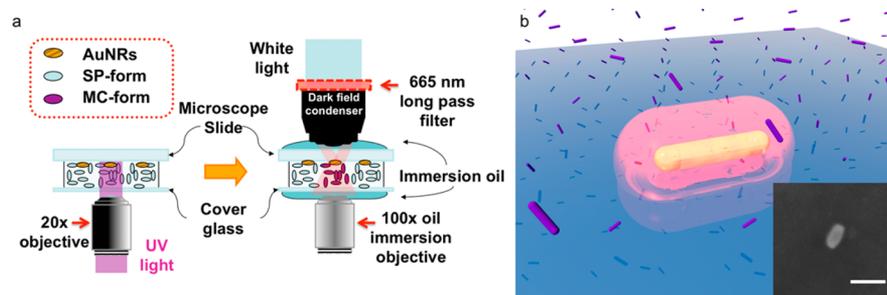

Figure 2. (a) Scheme of the sample and experimental setup for the study of PIRET by single-nanoparticle dark-field scattering spectroscopy. UV light induces SP−MC isomerization. (b) Schematics of a single AuNR covered with an MC-doped PMMA thin film (thickness is 580 nm) on a glass slide. The single golden rod represents the AuNR, the purple rods illustrate MC molecules, and the red color displays the PIRET-active volume. The inset in b is a representative SEM image of an individual AuNR on the substrate. Scale bar is 60 nm. More SEM images of AuNRs are provided in the Supporting Information (SI).
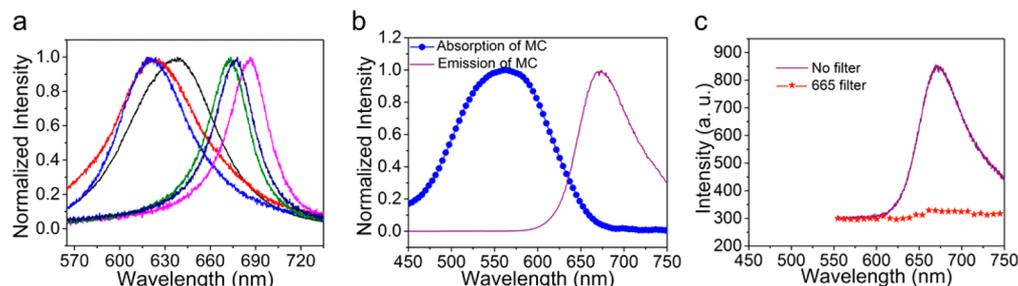
Figure 3. (a) Normalized single-nanoparticle scattering spectra for different AuNRs covered by pure PMMA films on substrates. (b) Normalized absorption and emission spectra of an MC-doped PMMA film measured by a standard fluorometer. The emission spectrum was excited at 390 nm. (c) Fluorescence spectra of an MC-doped PMMA film measured by dark-field optical spectroscopy without (purple) and with (red) the use of a 665 nm long-pass filter. White light was used as the excitation source. Data at short wavelengths are not available because of limitations of the grating in our spectroscopy.

(PMT) (H7422PA-40, Hamamatsu) in non-descanned detection scheme. Before reaching the photon-counting board (SPC-150, Becker and Hickl GmbH), the output current of the PMT is amplified via a preamplifier (HFAC-26, Becker and Hickl GmbH). The detailed information for FLIM setup can be found in a previous report.[13] A custom LabView interface was used to acquire data, while a custom Matlab script was used to process the FLIM data sets. Fluorescence lifetimes were recorded with an average laser power of 4 mW. The TCSPC bin resolution was 20 ps, and the FLIM pixel integration time was 5 ms. Lifetimes were fit at each pixel via a least-squares method using a single exponential decay model.[14]

RESULTS AND DISCUSSION

We used single-nanoparticle scattering spectroscopy based on dark-field optical microscopy to investigate molecular fluorescence via blue-shifted PIRET from single AuNRs to dye molecules. The experimental setup and samples are shown in Figure 2a and b. AuNRs were selected because of several considerations. AuNRs not only allow a high tunability of LSPR peak wavelengths,[9,10] but they also have a long dephasing time,[15] which can enhance the efficiency of energy transfer to dye molecules.[4] Additionally, the narrow spectral line width of AuNRs allows us to better distinguish the LSPR scattering peak from the emission peak of the dye. With a small detection volume and a high sensitivity toward local environmental variations, single-nanoparticle scattering spectroscopy can eliminate the inhomogeneity and averaging effects inherent to ensemble measurements, enabling accurate shape- and size-dependent studies of the optical properties of NPs.[16−24] Figure 2b and Figure S1a and S1b show SEM images of AuNRs. From Figure S1a and S1b, we can see that our AuNRs have different sizes and aspect ratios and thus can cover a range of LSPR peak wavelengths. The representative single-nanoparticle scattering spectra of different AuNRs covered by pure PMMA films are displayed in Figure 3a. We can see that the line width of the scattering spectra is reduced when the peak wavelength is ≥673 nm. This line width reduction is caused by the suppression of the interband damping in Au at longer wavelengths.[15] The interband damping of AuNRs, which has a threshold at the energy of ∼1.8 eV, is also the main reason that causes the variation of the spectrum line shape at wavelengths below 673 nm. Using single-nanoparticle spectroscopy, we managed to induce and measure blue-shifted PIRET by tuning the LSPR of AuNRs relative to the absorption and emission bands of adsorbed dye molecules at AuNRs, because PIRET efficiency strongly depends on the emission−absorption spectral overlap.[4]

Spiropyran (SP) molecules in their open form, which are known as merocyanine (MC), have a large Stokes shift between absorption and emission peak wavelengths, as shown in Figure 3b. Because of the difference in peak wavelength (ca. 100 nm) between the absorption and emission spectra of MC, the LSPR peak wavelength of AuNRs can be tuned to be separated from the emission band of MC while overlapping with its absorption band. As shown in Figure 2a, a single-nanoparticle scattering spectrum recorded with our dark-field optical spectroscopy covers the mixed signals from the LSPR scattering of AuNRs and the fluorescence of MC molecules, therefore becoming an ideal platform to study the effects of spectral overlap on the efficiency of blue-shifted PIRET. Our samples are submonolayers of well-separated AuNRs on glass substrates, covered by MC-doped PMMA films (Figure 2a). Optical measurements were made upon UV irradiation of the molecules and formation of MC isomers. The SP−MC photoisomerization is illustrated in Figure S2.

As schematically shown in Figure 1b, when the LSPR peak of AuNRs is located between the absorption and emission peaks of MC, the spectral overlap between the LSPR scattering (emission) and the absorption of MC molecules allows blue-shifted PIRET from AuNRs to MC. Meanwhile, the molecular emission band also overlaps with the LSPR absorption band, which enables red-shifted FRET from the molecules to AuNRs.[4] The net direction of energy transfer between AuNRs and MC molecules is determined by the dephasing time (T_2), which is given by[4,15,25]

$$\frac{1}{T_2} = \frac{1}{2T_1} + \frac{1}{T_2^*}$$ (1)

where T_1 is the recombination time that describes the relaxation from the excited state to the ground state in AuNRs (or dye molecules) and T_2^* is the pure dephasing time of AuNRs (or dye molecules). Since T_2^* is in the fs range and T_1 is in the ps range, T_2 is relevant to T_2^*.[25] When T_2^* of LSPRs is longer than that of molecular fluorescence, coherent excitons of molecules dephase more rapidly than the LSPRs of AuNRs do. Under this condition, PIRET is more efficient than FRET and energy transfers from the AuNRs to the molecules.[4]

On the basis of the dark-field optical microscopy study as described in Figure 2a, we measured the fluorescence spectra of MC molecules doped in the PMMA film under white-light excitation. Figure 3c shows the spectra with (indicated by "665 filter") and without (indicated by "No filter") the use of a 665 nm long-pass filter. The fluorescence spectrum without the filter matches well with the single-wavelength-excited emission
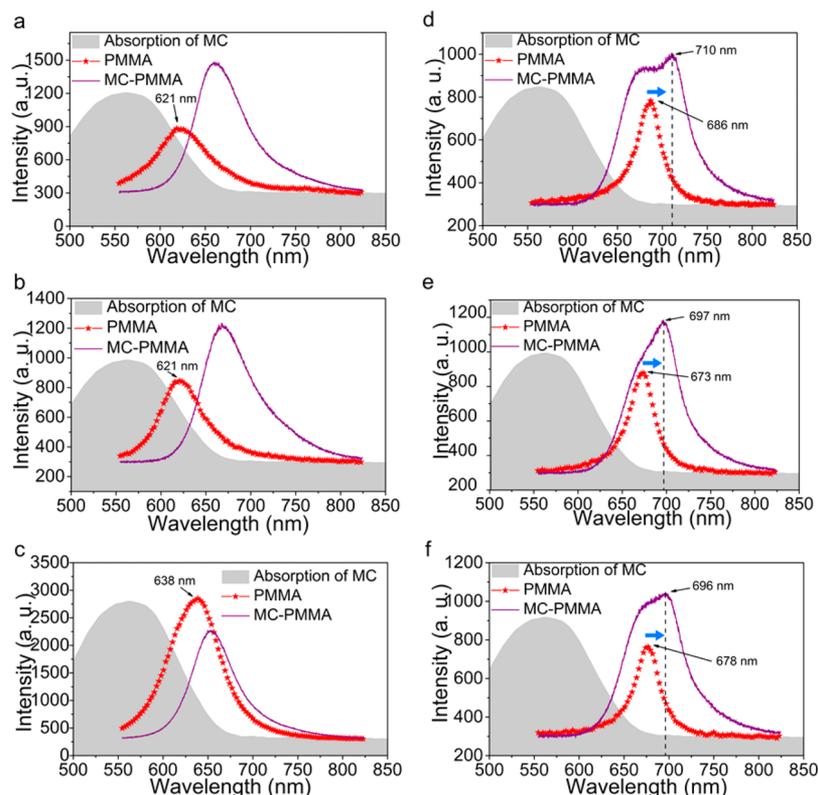
Figure 4. Single-nanoparticle spectra measured from AuNRs covered by MC-doped PMMA films or pure PMMA films when (a−c) the scattering spectra of AuNRs have large overlaps with the absorption band of MC molecules and (d−f) the scattering spectra of AuNRs have minimal overlap with the absorption of MC. The black arrows label the scattering LSPR peak positions, and the horizontal blue arrows in d−f indicate red shifts of the LSPR scattering peaks because of MC doping in PMMA. Also included are the absorption spectra of MC molecules measured by UV−vis−NIR spectroscopy.
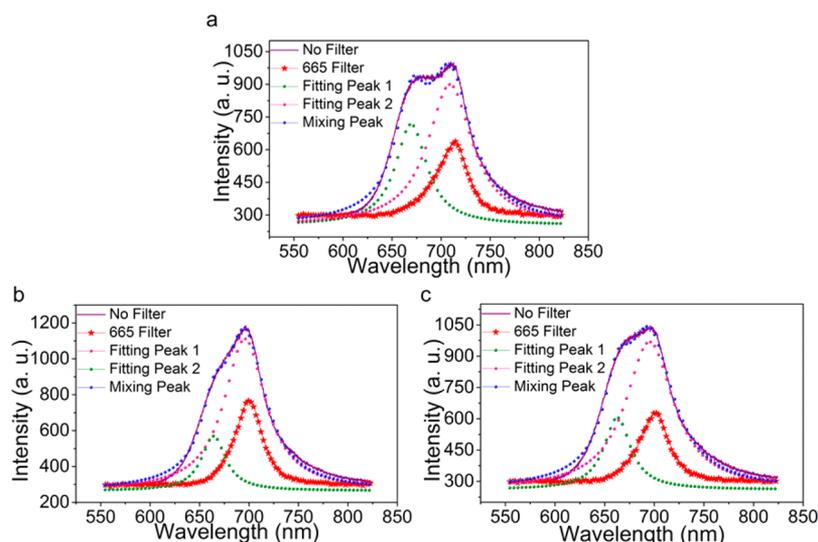

Figure 5. (a−c) Fitting the spectra with two peaks in Figure 4d−f with a Lorentzian model. The original spectra are indicated by "No filter". For each of the original spectra, the fitting leads to two Lorentzian peaks as indicated by "Fitting Peak 1" and "Fitting Peak 2". Cumulative spectra of two fitting spectra are indicated as "Mixing Peak". Also included is the scattering spectrum of a AuNR covered by the MC-doped PMMA film measured with the use of a 665 nm long-pass filter, as indicated by "665 filter".

spectrum from a standard fluorometer (Figure 3b). Both spectra exhibit the same fluorescence peak wavelength of 670 nm, confirming that dark-field optical spectroscopy allows us to excite and measure the fluorescence of MC molecules under white-light excitation. The capability of white light in exciting the fluorescence at a peak wavelength of 670 nm is also

supported by the excitation spectrum (Figure S3), which exhibits the strong excitation efficiency within the visible-light regime.

The use of a 665 nm long-pass filter, however, results in a significant reduction of the fluorescence of MC molecules (as indicated by the extremely weak spectrum in Figure 3c), which
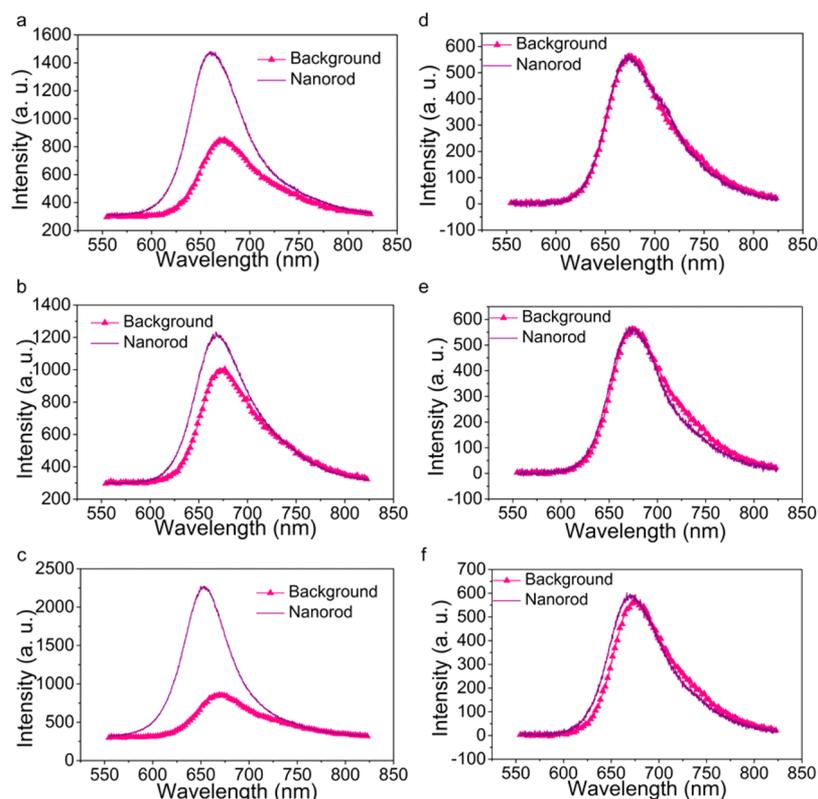
Figure 6. Fluorescence spectra from MC molecules at a AuNR (nanorod) and from molecules that are far away from the AuNR (background). (a–c) For the samples in Figure 4a–c, we observe enhanced fluorescence for the molecules at the AuNRs because of blue-shifted PIRET. (d–f) For the samples in Figure 4d–f, no obvious fluorescence enhancement is observed. The fluorescence spectra of molecules at the AuNR were obtained by subtracting the no filter spectra with the 665 filter spectra in Figure 5a–c.

will enable us to reveal the AuNR LSPR scattering component at the wavelengths longer than 665 nm from a mixture of fluorescence and scattering signals (Figure 4d–f). However, the use of the long-pass filter also significantly reduces the AuNR LSPR scattering when the peak wavelengths are shorter than the cutoff wavelength (i.e., 665 nm). To identify LSPR scattering peak wavelengths that are shorter than 665 nm, we measured the scattering spectra of the same AuNRs covered by either pure PMMA films or MC-doped PMMA films. By measuring AuNRs with different LSPRs under the same experimental conditions (more detailed information is provided in the Experimental Section), we observe two types of scenarios. The first scenario is shown in Figure 4a–c, where a single resonance peak (purple spectra) at ~670 nm is recorded for a AuNR covered by the MC-doped PMMA film. In this scenario, the scattering peak of the same AuNR covered by pure PMMA (red spectra in Figure 4a–c) significantly overlaps with the absorption band of MC molecules. The second scenario is illustrated in Figure 4d–f, where two peaks are observed in the spectrum of a AuNR covered by the MC-doped PMMA film. In this scenario, there is no obvious overlap between the scattering spectrum (red spectra in Figure 4d–f) of the same AuNR covered by pure PMMA films and the absorption band of MC molecules.

To better understand the two different scenarios in Figure 4a–f, we fitted the spectrum in Figure 4d–f into two individual peaks with the Lorentzian model. Taking Figure 5a as an example, the two Lorentzian peaks are at ~670 nm and ~710 nm. The ~670 nm peak is attributed to the molecular fluorescence. To further examine the origin of the 710 nm peak,

we measured the spectrum of the same AuNR covered by MC-doped PMMA film using a 665 nm long-pass filter. As a result, only the scattering peak of the AuNR at 715 nm is observed, as shown in Figure 5a, which matches well with the fitted peak at ~710 nm. Thus, we conclude that the two peaks in Figure 4d arise from both the fluorescence of MC molecules and the scattering of the AuNR. The same conclusion applies to other similar AuNRs, as shown in Figure 4e and f. As indicated by the blue arrows in Figure 4d–f, MC molecules in the PMMA film cause a red shift in the scattering peak, as compared to that of the AuNR covered by pure PMMA film, which may be attributed to the increased refractive index of the PMMA film in the presence of MC molecules. In other words, at the LSPR peak wavelengths of the AuNRs in Figure 4d–f, the refractive index of MC-doped PMMA films is larger than that of pure PMMA films and SP-doped PMMA films. An increase in the refractive index of the surrounding medium next to AuNRs leads to a red shift in their LSPRs. In the previous studies, similar red shifts occurred to the LSPR peak wavelengths of metal NPs when the SP was isomerized into MC in the PMMA.[26,27] In our hybrid system, the red shift further reduces the overlap between the LSPR band and the absorption band of the MC molecules.

The disappearance of the scattering peak in the first scenario (Figure 4a–c) indicates that there is energy transfer from the AuNR to MC molecules, which quenches the AuNR LSPR. The experimental observation confirms that the blue-shifted PIRET from AuNRs to MC can occur when the LSPR band overlaps the absorption band of the molecules. Meanwhile, the red-shifted FRET from MC to AuNRs can coexist with the
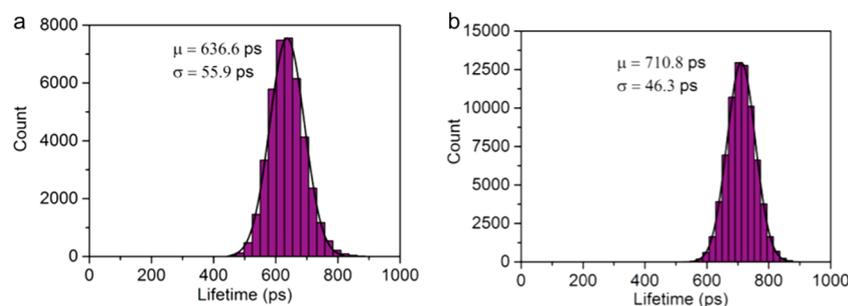
Figure 7. (a) Fluorescence lifetime of the MC-doped PMMA films. (b) Fluorescence lifetime of the MC-doped PMMA films with AuNRs where the LSPR spectrum overlaps with the molecular absorption spectrum.

PIRET since there is also an overlap between the LSPR band and the emission band. When the pure dephasing time of LSPRs of AuNRs (>10 fs) is larger than that of MC molecules,[15] the net energy transfer is from AuNRs to MC molecules, quenching the LSPR scattering.[4]

Besides the quenching of LSPR scattering, the resonance energy transfer is expected to enhance the molecular fluorescence.[12,28] We observe the fluorescence enhancement for MC molecules when the AuNR LSPR scattering band overlaps the emission band of MC molecules (Figure 6a−c). However, as shown in Figure 6d−f, no fluorescence enhancement occurs to MC molecules at the AuNRs in Figure 4d−f. Such a lack of fluorescence enhancement is consistent with the fact that the sample does not support blue-shifted PIRET because there is no overlap between LSPR and molecular absorption. The observed differences between Figure 6a−c and Figure 6d−f indicate that blue-shifted PIRET plays a critical role in the enhanced fluorescence of MC molecules. We also employed fluorescence lifetime imaging microscopy on the basis of time-correlated single photon counting to measure the fluorescence lifetime of MC-doped PMMA films with and without AuNRs. The LSPR of these AuNRs overlaps with the molecular absorption band. More details on the measurements are provided in the Experimental Section. As shown in Figure 7a and b, the average fluorescence lifetime (710.8 ± 46.3 ps) of MC-doped PMMA films with AuNRs is longer than that (636.6 ± 55.9 ps) for films without AuNRs. The increase of the average fluorescence lifetime further manifests that energy is transferred from AuNRs to MC molecules. It has been previously reported that energy transfer from donors to acceptors may increase the lifetime of acceptors.[12,29]

Furthermore, we can rule out the contribution of radiative-rate modification via Purcell effect to the fluorescence enhancement.[30−32] The different results for the samples in Figure 6a−c and Figure 6d−f indicate that fluorescence enhancement occurs only when there are emission−absorption spectral overlaps, as discussed in Figure 1b and c. However, radiative-rate enhancement via Purcell effect does not require the emission−absorption spectral overlap, which indicates that the Purcell effect is not a major factor in our fluorescence measurements.[30−32]

We further consider the differences in optical properties between AuNRs and dye molecules to identify the advantages of AuNRs over dye molecules as donors in resonant energy transfer. Compared with dye molecules, AuNRs have a larger absorption cross section (4−5 orders larger than that of conventional dyes).[8] In addition, when the donor−acceptor distance increases, the energy-transfer efficiency (Φ_{EnT}) of PIRET decays more slowly than that of FRET between two

fluorophores.[11] The energy-transfer efficiency (Φ_{EnT}) between the donor and the acceptor follows the equation[11,12,28,33]

$$\Phi_{EnT} = \frac{1}{1 + \left(\frac{R}{R_0}\right)^n} \tag{2}$$

where R is the donor−acceptor distance, R_0 is the characteristic distance at which Φ_{EnT} is 50%, and n is 4 and 6 for PIRET and FRET, respectively, which indicates that the Φ_{EnT} in PIRET decreases more slowly than that in FRET when R increases.[11,12,28,33] Additional details are available in the SI. Therefore, both the larger absorption cross section of AuNRs and the slower decay of energy-transfer efficiency as a function of increased donor−acceptor distance lead to a larger amount of energy transfer through PIRET than that through FRET.

There should be much larger fluorescence enhancement than our experimental measurements as shown in Figure 6a−c. This is because PIRET occurs within the volume near the AuNRs, which is much smaller than that from which fluorescence signals were measured. This highly confined volume accounts for a small fraction of the total volume where the light signals were collected in our dark-field optical microscope since there is a dramatic decrease in the PIRET efficiency (Φ_{PIRET}) between the AuNR and the molecules when the separation distance (R) increases (eq 2).[11,33] However, it has remained challenging to calculate the actual average enhancement factor (EF) because of the difficulty in determining R_0, which is needed for the calculation of the PIRET-active volume in our system. Instead, we estimated a conservative average EF of up to 1854 by using the largest PIRET-active volume according to previous studies.[4,11,33,34] As per previous studies,[4,11,34] the energy transfer between dye molecules and a Au nanoparticle is limited in the volume near the particle where the donor−acceptor distance is smaller than 50 nm. To estimate the average enhancement factors (EFs), we assume that the PIRET is limited in a volume within a distance of 50 nm[4,11,34] from the surfaces of AuNRs (Figure 2b and Figure 8a and b) and that the MC concentration is uniform in PMMA. The average EF is defined by
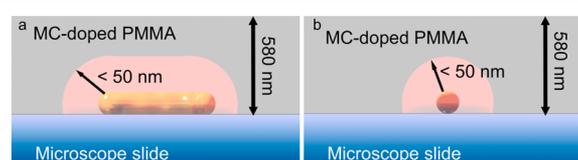

Figure 8. Cross-sectional view along the (a) long axis and (b) short axis of the AuNR in Figure 2b.

$$EF = \left(\frac{P_{\text{AuNRs}}}{P_{\text{background}}} \right) \left(\frac{V_{\text{background}}}{V_{\text{AuNRs}}} \right) \tag{3}$$

where P_{AuNRs} is the enhanced fluorescence intensity from MC molecules within the distance of 50 nm from the surfaces of AuNRs. The P_{AuNRs} is the difference between the integrated intensities of fluorescence spectra with and without a AuNR. $P_{\text{background}}$ is the integrated intensity of the fluorescence spectrum without AuNRs. V_{AuNRs} is the PIRET-active volume, as indicated by red color in Figure 2b and Figure 8a and b. $V_{\text{background}}$ is the total volume from which we collected the fluorescence signals (1.92 μm × 1.92 μm × 580 nm). To calculate V_{AuNRs}, we use the largest dimensions (25 nm diameter × 73 nm length) and volumes of AuNRs from the data provided by the company that sold the AuNRs (see Experimental Section). On the basis of Figure 6c, we obtain the maximum average EF of 1854. Since the average $EF \propto 1/V_{\text{AuNRs}}$, the average EF is underestimated because of the use of the maximum volume of the AuNRs. The variations in average EFs among different AuNRs and samples can be attributed to the variations in the MC concentrations. In contrast, we can see from Figure 6c−f that FRET hardly changes the fluorescence intensity because of the small amount of MC molecules involved in the process.

CONCLUSIONS

In summary, we have demonstrated molecular fluorescence enhancement through blue-shifted PIRET from single AuNRs to dye molecules. PIRET and fluorescence enhancement occur only when there is a significant spectral overlap between the light scattering of AuNRs and the absorption of MC molecules. The fluorescence enhancement indicates that AuNRs can function as donors to enhance the fluorescence excitation of acceptors. AuNRs have two major advantages over dye molecules as donors: larger absorption cross section and slower decay of energy transfer efficiency via donor−acceptor distance. Both effects lead to a lower intensity requirement for the incident light. Moreover, the blue-shifted PIRET allows the excitation of fluorescence of molecules near metal NPs using light of lower energy (i.e., longer wavelength). Therefore, blue-shifted PIRET provides a new pathway toward the design of NP−dye pairs for biosensing and bioimaging, with low excitation energy and high signal-to-noise ratio. In addition, the white-light excitation of both the fluorescence of dye molecules and the LSPRs of single AuNPs will enable the multiplexed sensing or imaging with different types of NP−dye pairs, using a dark-field microscope.

ASSOCIATED CONTENT

Ⓢ Supporting Information

The Supporting Information is available free of charge on the ACS Publications website at DOI: 10.1021/acs.jpcc.6b04205.

> The fluorescence of MC molecules, the morphology of AuNRs, the schematic of SP−MC photoisomerization, the excitation spectrum of MC molecules, and the relationship between the PIRET efficiency and the donor−acceptor distance
> (PDF)

AUTHOR INFORMATION

Corresponding Author
*E-mail: zheng@austin.utexas.edu.

Notes

The authors declare no competing financial interest.

ACKNOWLEDGMENTS

REFERENCES

(1) Liu, G. L.; Long, Y.-T.; Choi, Y.; Kang, T.; Lee, L. P. Quantized Plasmon Quenching Dips Nanospectroscopy via Plasmon Resonance Energy Transfer. *Nat. Methods* **2007**, *4*, 1015−1017.

(2) Choi, Y.; Kang, T.; Lee, L. P. Plasmon Resonance Energy Transfer (PRET)-based Molecular Imaging of Cytochrome *c* in Living Cells. *Nano Lett.* **2009**, *9*, 85−90.

(3) Choi, Y.; Park, Y.; Kang, T.; Lee, L. P. Selective and Sensitive Detection of Metal Ions by Plasmonic Resonance Energy Transfer-Based Nanospectroscopy. *Nat. Nanotechnol.* **2009**, *4*, 742−746.

(4) Li, J.; Cushing, S. K.; Meng, F.; Senty, T. R.; Bristow, A. D.; Wu, N. Plasmon-Induced Resonance Energy Transfer for Solar Energy Conversion. *Nat. Photonics* **2015**, *9*, 601−607.

(5) Cushing, S. K.; Li, J.; Meng, F.; Senty, T. R.; Suri, S.; Zhi, M.; Li, M.; Bristow, A. D.; Wu, N. Photocatalytic Activity Enhanced by Plasmonic Resonant Energy Transfer from Metal to Semiconductor. *J. Am. Chem. Soc.* **2012**, *134*, 15033−15041.

(6) Cushing, S. K.; Li, J.; Bright, J.; Yost, B. T.; Zheng, P.; Bristow, A. D.; Wu, N. Controlling Plasmon-Induced Resonance Energy Transfer and Hot Electron Injection Processes in Metal@TiO2 Core−Shell Nanoparticles. *J. Phys. Chem. C* **2015**, *119*, 16239−16244.

(7) Li, J.; Cushing, S. K.; Zheng, P.; Meng, F.; Chu, D.; Wu, N. Plasmon-Induced Photonic and Energy-Transfer Enhancement of Solar Water Splitting by a Hematite Nanorod Array. *Nat. Commun.* **2013**, *4*, 2651.

(8) Jain, P. K.; Lee, K. S.; El-Sayed, I. H.; El-Sayed, M. A. Calculated Absorption and Scattering Properties of Gold Nanoparticles of Different Size, Shape, and Composition: Applications in Biological Imaging and Biomedicine. *J. Phys. Chem. B* **2006**, *110*, 7238−7248.

(9) Hu, M.; Chen, J.; Li, Z.-Y.; Au, L.; Hartland, G. V.; Li, X.; Marquez, M.; Xia, Y. Gold Nanostructures: Engineering Their Plasmonic Properties for Biomedical Applications. *Chem. Soc. Rev.* **2006**, *35*, 1084−1094.

(10) Chen, H.; Shao, L.; Li, Q.; Wang, J. Gold Nanorods and Their Plasmonic Properties. *Chem. Soc. Rev.* **2013**, *42*, 2679−2724.

(11) Yun, C. S.; Javier, A.; Jennings, T.; Fisher, M.; Hira, S.; Peterson, S.; Hopkins, B.; Reich, N. O.; Strouse, G. F. Nanometal Surface Energy Transfer in Optical Rulers, Breaking the FRET Barrier. *J. Am. Chem. Soc.* **2005**, *127*, 3115−3119.

(12) Clapp, A. R.; Medintz, I. L.; Mattoussi, H. Förster Resonance Energy Transfer Investigations Using Quantum-Dot Fluorophores. *ChemPhysChem* **2006**, *7*, 47−57.

(13) Perillo, E. P.; Liu, Y.-L.; Huynh, K.; Liu, C.; Chou, C.-K.; Hung, M.-C.; Yeh, H.-C.; Dunn, A. K. Deep and High-Resolution Three-Dimensional Tracking of Single Particles Using Nonlinear and Multiplexed Illumination. *Nat. Commun.* **2015**, *6*, 7874.

(14) Warren, S. C.; Margineanu, A.; Alibhai, D.; Kelly, D. J.; Talbot, C.; Alexandrov, Y.; Munro, I.; Katan, M.; Dunsby, C.; French, P. M. W. Rapid Global Fitting of Large Fluorescence Lifetime Imaging Microscopy Datasets. *PLoS One* **2013**, *8*, e70687.

(15) Sönnichsen, C.; Franzl, T.; Wilk, T.; von Plessen, G.; Feldmann, J.; Wilson, O.; Mulvaney, P. Drastic Reduction of Plasmon Damping in Gold Nanorods. *Phys. Rev. Lett.* **2002**, *88*, 077402.

(16) Ringe, E.; Sharma, B.; Henry, A.-I.; Marks, L. D.; Van Duyne, R. P. Single Nanoparticle Plasmonics. *Phys. Chem. Chem. Phys.* **2013**, *15*, 4110−4129.

(17) Rajeeva, B. B.; Hernandez, D. S.; Wang, M.; Perillo, E.; Lin, L.; Scarabelli, L.; Pingali, B.; Liz-Marzán, L. M.; Dunn, A. K.; Shear, J. B.; et al. Regioselective Localization and Tracking of Biomolecules on Single Gold Nanoparticles. *Adv. Sci.* **2015**, *2*, 1500232.

(18) Ni, W.; Ambjörnsson, T.; Apell, S. P.; Chen, H.; Wang, J. Observing Plasmonic-Molecular Resonance Coupling on Single Gold Nanorods. *Nano Lett.* **2010**, *10*, 77−84.

(19) Anker, J. N.; Hall, W. P.; Lyandres, O.; Shah, N. C.; Zhao, J.; Van Duyne, R. P. Biosensing with Plasmonic Nanosensors. *Nat. Mater.* **2008**, *7*, 442−453.

(20) Ming, T.; Zhao, L.; Yang, Z.; Chen, H.; Sun, L.; Wang, J.; Yan, C. Strong Polarization Dependence of Plasmon-Enhanced Fluorescence on Single Gold Nanorods. *Nano Lett.* **2009**, *9*, 3896−3903.

(21) Ming, T.; Zhao, L.; Xiao, M.; Wang, J. Resonance-Coupling-Based Plasmonic Switches. *Small* **2010**, *6*, 2514−2519.

(22) McFarland, A. D.; Van Duyne, R. P. Single Silver Nanoparticles as Real-Time Optical Sensors with Zeptomole Sensitivity. *Nano Lett.* **2003**, *3*, 1057−1062.

(23) Sherry, L. J.; Jin, R.; Mirkin, C. A.; Schatz, G. C.; Van Duyne, R. P. Localized Surface Plasmon Resonance Spectroscopy of Single Silver Triangular Nanoprisms. *Nano Lett.* **2006**, *6*, 2060−2065.

(24) Sherry, L. J.; Chang, S.-H.; Schatz, G. C.; Van Duyne, R. P.; Wiley, B. J.; Xia, Y. Localized Surface Plasmon Resonance Spectroscopy of Single Silver Nanocubes. *Nano Lett.* **2005**, *5*, 2034−2038.

(25) Link, S.; El-Sayed, M. A. Size and Temperature Dependence of the Plasmon Absorption of Colloidal Gold Nanoparticles. *J. Phys. Chem. B* **1999**, *103*, 4212−4217.

(26) Dintinger, J.; Klein, S.; Ebbesen, T. W. Molecule-Surface Plasmon Interactions in Hole Arrays: Enhanced Absorption, Refractive Index Changes, and All-Optical Switching. *Adv. Mater.* **2006**, *18*, 1267−1270.

(27) Zheng, Y. B.; Kiraly, B.; Cheunkar, S.; Huang, T. J.; Weiss, P. S. Incident-Angle-Modulated Molecular Plasmonic Switches: A Case of Weak Exciton−Plasmon Coupling. *Nano Lett.* **2011**, *11*, 2061−2065.

(28) Sapsford, K. E.; Berti, L.; Medintz, I. L. Materials for Fluorescence Resonance Energy Transfer Analysis: Beyond Traditional Donor-Acceptor Combinations. *Angew. Chem., Int. Ed.* **2006**, *45*, 4562−4589.

(29) Kagan, C. R.; Murray, C. B.; Nirmal, M.; Bawendi, M. G. Electronic Energy Transfer in CdSe Quantum Dot Solids. *Phys. Rev. Lett.* **1996**, *76*, 1517−1520.

(30) Anger, P.; Bharadwaj, P.; Novotny, L. Enhancement and Quenching of Single-Molecule Fluorescence. *Phys. Rev. Lett.* **2006**, *96*, 113002.

(31) Rose, A.; Hoang, T. B.; McGuire, F.; Mock, J. J.; Ciracì, C.; Smith, D. R.; Mikkelsen, M. H. Control of Radiative Processes Using Tunable Plasmonic Nanopatch Antennas. *Nano Lett.* **2014**, *14*, 4797−4802.

(32) Akselrod, G. M.; Argyropoulos, C.; Hoang, T. B.; Ciracì, C.; Fang, C.; Huang, J.; Smith, D. R.; Mikkelsen, M. H. Probing the Mechanisms of Large Purcell Enhancement in Plasmonic Nanoantennas. *Nat. Photonics* **2014**, *8*, 835−840.

(33) Sen, T.; Sadhu, S.; Patra, A. Surface Energy Transfer from Rhodamine 6G to Gold Nanoparticles: A Spectroscopic Ruler. *Appl. Phys. Lett.* **2007**, *91*, 043104.

(34) Griffin, J.; Singh, A. K.; Senapati, D.; Rhodes, P.; Mitchell, K.; Robinson, B.; Yu, E.; Ray, P. C. Size- and Distance-Dependent Nanoparticle Surface-Energy Transfer (NSET) Method for Selective Sensing of Hepatitis C Virus RNA. *Chem. - Eur. J.* **2009**, *15*, 342−351.